How do the Mutations in *Pf*K13 Protein Promote Anti-malarial Drug Resistance ?

Shikha Sharma and Md. Ehesan Ali*

Institute of Nano Science and Technology, Sector-81, Mohali, Punjab-140306, India

E-mail: ehesan.ali@inst.ac.in

Abstract

Plasmodium falciparum develops resistance to artemisinin upon exposure to the anti-malarial drug. Various mutations in the *Plasmodium falciparum* Kelch13 (*Pf*K13) protein such as Y493H, R539T, I543T, and C580Y have been associated with anti-malarial drug resistance. (Ariey et al., *Nature*, **2**014, *505*, 50-55) These mutations impede the regular ubiquitination process that eventually invokes drug resistance. However, the relationship between the mutation and the mechanism of drug resistance has not yet been fully elucidated. The comparative protein dynamics are studied by performing the classical molecular dynamics (MD) simulations and subsequent analysis of the trajectories adopting root-means-square fluctuations, the secondary-structure predictions and the dynamical cross-correlation matrix analysis tools. Here we observed that the mutations in the Kelch-domain does not have any structural impact on the mutated site, however it significantly alters the overall dynamics of the protein. The loop-region of the BTB-domain especially for Y493H and C580Y mutants, are found to have the enhanced dynamical fluctuations. The enhanced fluctuations in the BTB-domain could affect the protein-protein (*Pf*K13-Cullin) binding interactions in the ubiquitination process and eventually leads to anti-malarial drug resistance.

1 Introduction

Artemisinin and its derivatives are the most effective and widely used treatment for *Plasmodium falciparum* malaria. The emergence and spread of drug resistance in the malaria parasite is a severe public health concern all over the malaria-endemic countries.[1–3] Artemisinin resistance is defined as delayed parasite clearance following treatment with artemisinin monotherapy or with artemisinin-based combination therapy.[4–6] Early signs of delayed response to artemisinin in *Plasmodium falciparum* parasite were first reported in 2009 in northwest Cambodia.[7,8] This phenotype has been now reported in Thailand,[8,9] Vietnam,[10,11] Myanmar,[8,12] and China.[13] Resistance to artemisinin has also been reported in India,[14,15] and is highly suspected in South America[16] and East Africa.[17,18]

Single site mutations in the *Plasmodium falciparum* Kelch13 protein (*Pf*K13) were associated with the artemisinin resistance.[19–21] Till now, 124 different non-synonymous kelch mutations have been identified which are associated with the artemisinin resistance.[22–24] The frequent and most prevalent mutations detected in resistant populations are Y493H (tyrosine(Y) @493 is replaced by histidine(H)), R539T (arginine(R) @539 is replaced by threonine(T)), I543T (isoleucine(I) @543 is replaced by threonine(T)) and C580Y (cysteine(C) @580 is replaced by tyrosine(Y)) respectively.[24–26] The C580Y mutation occurs in about 55% of samples with any resistance mutation in Southeast Asia and is assumed to be one of the strong molecular markers for artemisinin resistance.[25] The next most prevalent mutation is Y493H, which occurs in about 10% of samples with any resistance mutation in Southeast-Asia.[27]

The *Pf*K13 protein contains 726 amino-acid residues consisting of non-conserved apicomplexa-specific N-terminal region (amino-acids 1-211), highly conserved coiled-coil-containing domain (amino-acids 212–341), well-conserved BTB-domain (amino-acids 350-442) and C-terminal Kelch-domain (amino-acids 443-726) as shown in Fig.1b. The Kelch-domain (propeller domain) has six kelch motifs and the mutations are present in this propeller domain

(Fig.1a). The BTB-domain interacts with cullin protein and gets involved in protein-protein interactions.[28–31] However, the Kelch domain acts as a receptor for substrate proteins to be ubiquitinated.[32–34]

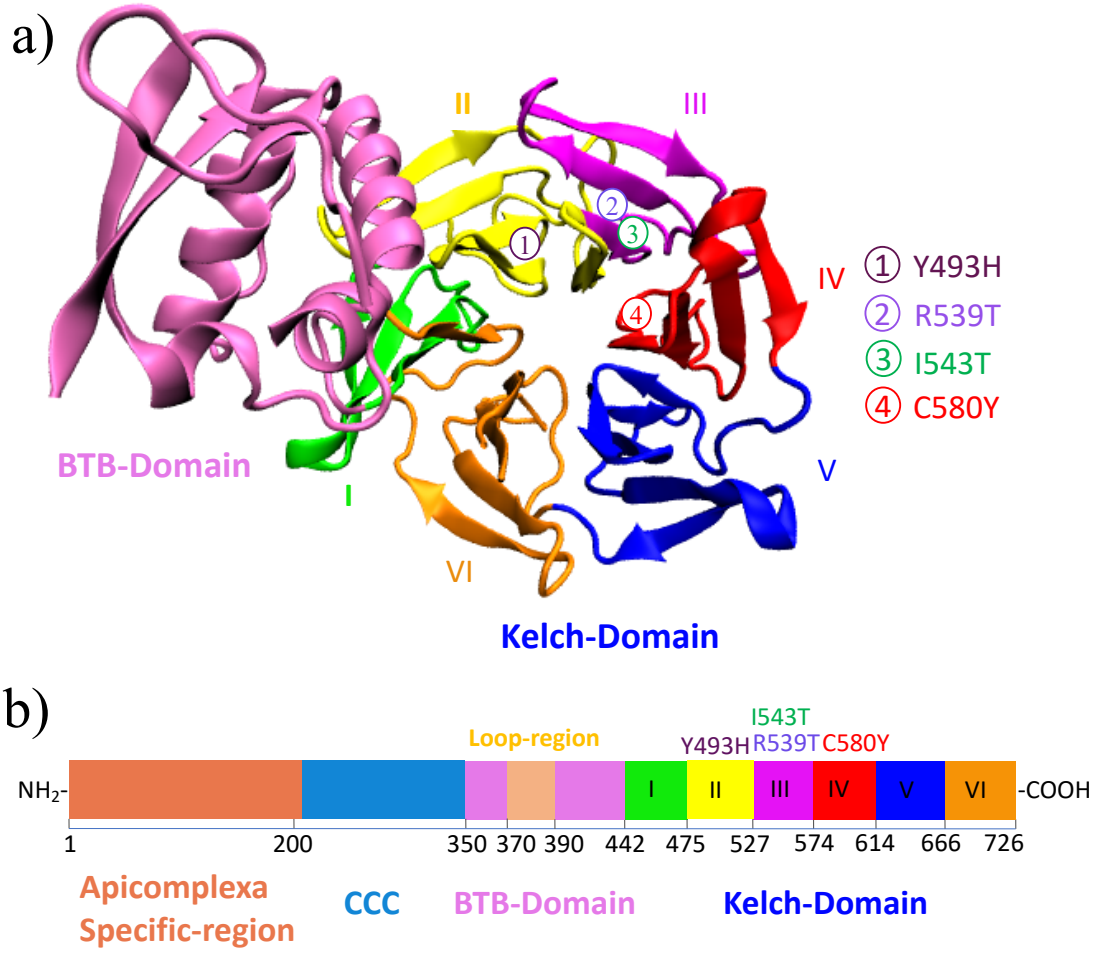

Figure 1: Structure of *Plasmodium falciparum* Kelch13 (*Pf*K13) protein. (a) PfKelch13 contains the BTB-domain at the amino terminus of proteins and the Kelch-domain that contains multiple kelch repeats. The location of the various mutations is indicated by spheres, where Y493h mutation resides in the blade II, I543T and R539T mutation are in blade III and C580Y mutation in blade IV. (b) PfK13 domain annotation, 1 to 211 amino-acid residues sequence is the poorly conserved plasmodium specific region, 212 to 341 is the coiled-coil-containing domain, 350 to 442 is the BTB specific sequence and 442 to 726 have kelch repeat sequence.

The proposed mechanism of artemisinin resistance is the proteostatic dysregulation of *Plasmodium falciparum* Phosphatidylinositol-3-Kinases (*Pf*PI3K) enzyme.[35] By binding to *Pf*PI3K enzymes, *Pf*K13 leads to its ubiquitination and degradation. Mutation in the *Pf*K13

prevents this interaction, thus increasing the levels of *Pf*PI3K enzyme and its product phosphatidylinositol 3-phosphate, subsequently leading to artemisinin resistance.[36,37]

A large number of *Pf*K13 mutations have been associated with artemisinin resistance,[19,21,26] however, it is not yet known why do these specific mutations instigate drug resistance. In this work, we have investigated the structural dynamics of *Pf*K13 wild-type (WT) and four mutant protein structures by adopting the classical molecular dynamic simulations[38–40] to address the issue and established a correlation of the protein dynamics with the artemisinin drug resistance.

2 Computational Methodology

To perform the classical molecular dynamics for *Pf*K13, the initial coordinates were obtained from the reported crystal structure (PDB ID:4yy8).[41] For the mutant structures, all the four mutants were generated using the mutagenesis function of Pymol by substituting the residue with the mutant residue.[42] Simulations were performed on the monomeric state of *Pf*K13, using the NAMD simulation package.[43,44] AMBER FF14SB force-field was used to generate the force fields of WT and mutant structures.[45] The systems were immersed in the cubic box of TIP3P water molecules maintaining at least 15Å of the separation between the solute and the edges of the box.[46] The system was centred in the periodic box of dimensions of 90.53 x 118.56 x 84.13 $Å^3$ containing 23190 water molecules. The $10Na^+$ and $6Cl^-$ counter ions were added to the water to make the overall charge neutrality of the system. The Particle Mesh Ewald (PME) approach was employed for the long-range interactions and a cut-off value of 10Å were used for the short-range interactions.[47] The system was minimized at 0K for 0.1ns keeping the heavy atoms fixed. Further, the system was equilibrated at a constant temperature, i.e., at 300K and 1 atm pressure for 0.25ns. The simulation was carried out under NPT ensembles for 400ns. The initial 200ns were performed as equilibration by removing the constraint force and allowing the free movement of the atoms. Subsequently, 200ns were

treated as production dynamics for the structural analysis. The resulting trajectories were visualized and analyzed using the VMD software.[48]

3 Results and Discussion

To understand the protein dynamics of WT and mutant structures we have performed the comparative analysis of the simulated trajectories utilizing the various computational tools. The details are discussed in the following sections. The secondary structure predictions and DCCM analysis have been discussed in the subsequent subsections.

3.1 Comparison of protein dynamics of WT and mutants

In order to obtain the comparative protein dynamics, we have performed the root-mean square-deviation (RMSD) analysis of the simulated individual five trajectories (one WT and four mutant-type). The domain-wise analysis (Kelch-domain, BTB-domain and Loop-region) has been performed and compared with the complete-protein (see Fig.1). The RMSD plots for all the five trajectories are given in Fig.2.

In all the mutants, the mutation sites are located within the Kelch-domain only. However, the comparisons of the RMSDs for the Kelch-domain do not indicate any significant change in the RMSD fluctuations. It is expected to observe significantly different fluctuations in the mutated regions in comparison to the WT. The RMSD fluctuations for the Kelch-domain are quite small throughout the simulation for all the cases and the average value of RMSD ranges from 0.88Å to 1.11Å. For the Y493H it is 0.88Å. This indicates that Y493H has significantly less fluctuations for the Kelch-domain compared to WT and other mutant proteins. Further investigations reveal that a non-covalent electrostatic interaction between the His493 and Glu426 induces compactness in the Kelch-domain in Y493H. We also compared the pore diameter of Kelch-Domain to further investigate the compactness of the protein (Fig.S1). It revealed that Y493H indeed possesses the smallest pore of 9.7Å compared to the average

value of 10.3Å for all the other cases .

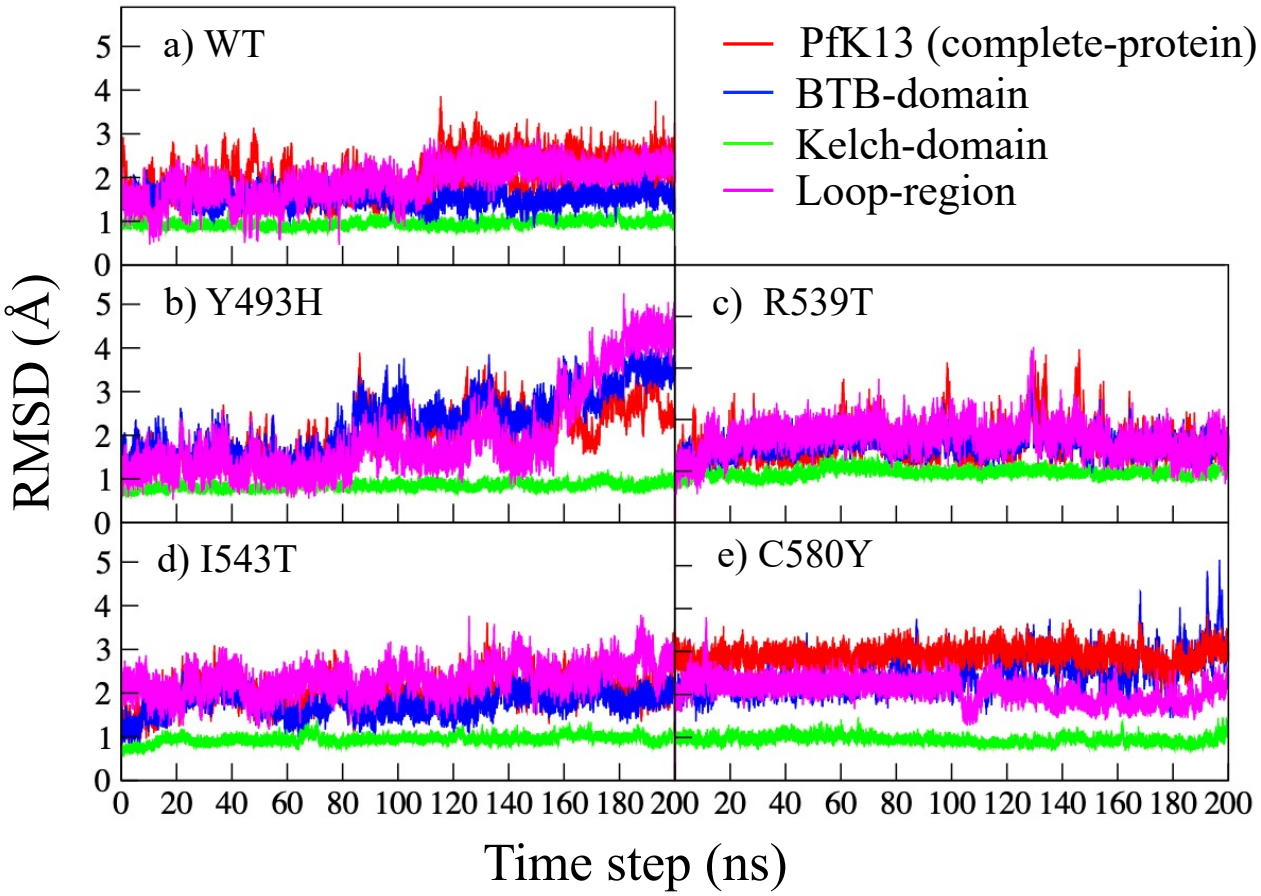

Figure 2: Calculated RMSD for the WT and mutant structures. The domain-wise fluctuations are shown for all the cases. The Kelch-domain shows a small and constant RMSD value for all the structures (green), while higher fluctuations are seen in the loop-region of the BTB-domain (pink). The large fluctuation in the BTB-domain (blue) and PfK13 (red) is also shown for the WT and mutants. A very high structural deviation is seen in the Y493H as well as in the C580Y.

Further, we observed quite large fluctuations in the BTB-domain, especially at the N-terminal region for all the cases. The average value of the RMSD fluctuations for heavy atoms in the BTB-domain for all the cases ranges from 2.11Å to 3.24Å. The average RMSD value for the WT is 2.26Å (Fig.2a) however, it is 2.11Å for the R539T which is the lowest value among all the mutants (Fig.2c).

In Y493H, we have observed quite a rich feature in the RMSD plot due to conformation change in the protein. The average RMSD value of 1.45Å is observed in the corresponding

trajectory up to 85ns, and then the switching of the confirmation occurs. Subsequently, other conformational changes are observed at 155ns (Fig.2b). The primary reason behind these confirmation switches is the change in the protein's secondary structure, which has been described in section 3.3. The RMSD value increases when going from the turns to coils. The signature of the conformation change is captured in the probability distribution plot as well. (See Fig.3c) Three different peaks are observed for Y493H with the RMSD values of 1.45, 2.46 and 3.33Å and each peak corresponds to the three different conformations.

In C580Y, we have seen the different scenarios in the RMSD plot, where the large fluctuations are observed for the complete-protein rather than the BTB-domain (Fig.2e). The average RMSD value of the complete-protein is 2.55 Å. The probability distribution of RMSD also indicates the broader peak for the complete protein (Fig.3a). It reveals that the higher fluctuation in this particular mutant is due to the loss of hydrogen-bond interaction between Cys580-Gly533 residues (Fig.S3). No large fluctuations are observed in the R539T and I543T mutants.

It has been observed that among four mutants, there are larger fluctuations in the dynamics of the BTB-domain of Y493H and C580Y as compared to the WT. Even though both of the mutants have larger fluctuations in the BTB-domain than the WT but the microscopic details of the dynamics of C580Y and Y493H are completely different from each other. It has been observed that the mutation in the Kelch domain does not have any local impact but it has a large impact on the overall structure and dynamics of the BTB-domain as well as on the loop-region of the BTB-domain.

We further analysed the effect of mutations on the compactness of the protein by calculating the radius of gyration (Rg). The average Rg value in between the range of 22.18 to 23.12 Å is obtained for all the cases Fig.S2. The average Rg value for the Y493H is calculated as 22.18 Å. The decrease in Rg value for Y493H is responsible for the overall compactness in this particular protein.

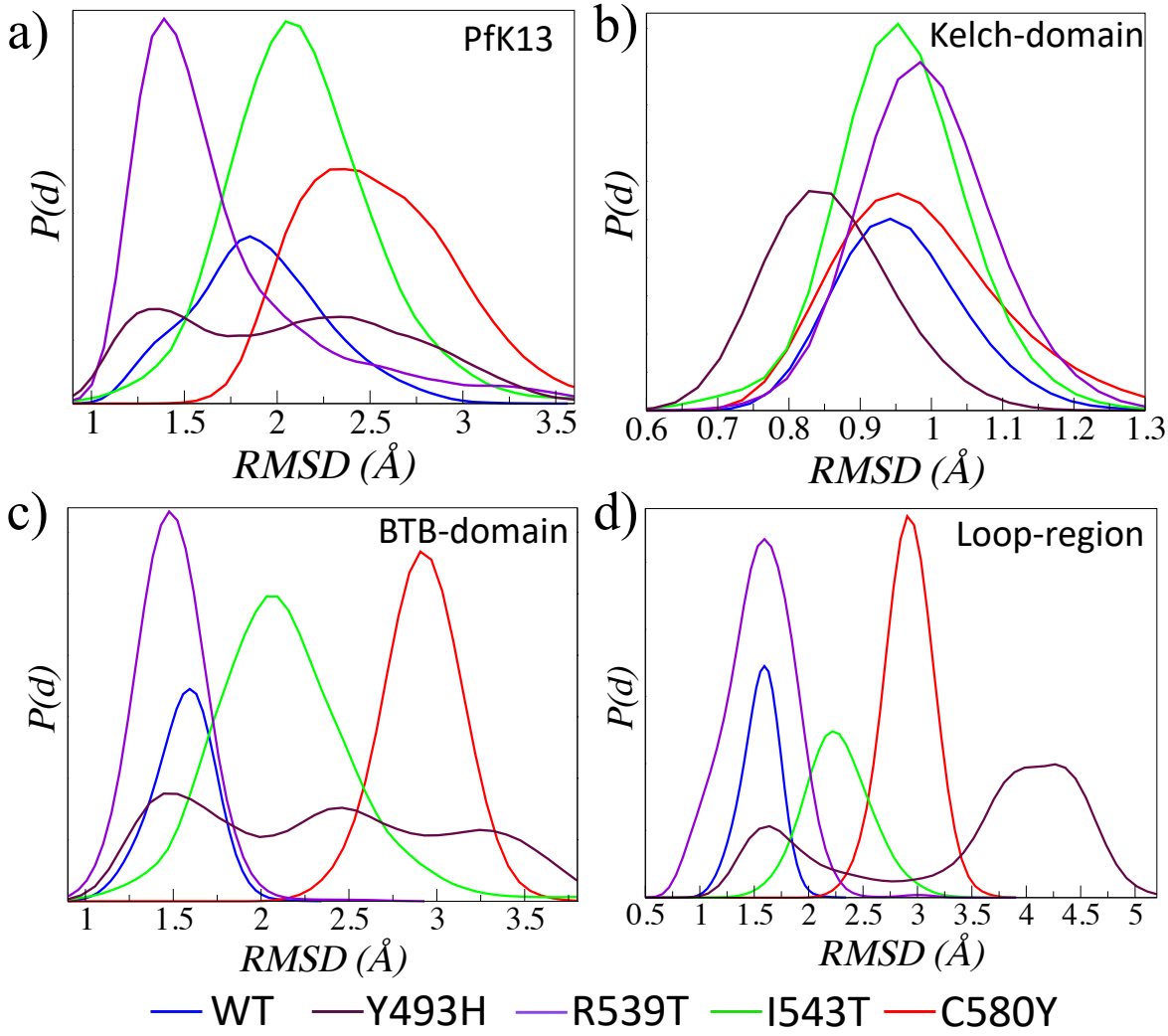

Figure 3: The conformational probability distribution plots of the different domains of PfKelch13 protein as a function of the backbone RMSD (a) In PfK13, the RMSD shows uni-model distribution with the single-peak for all the cases except Y493H which has bi-model distribution with two peaks. (b) In Kelch-domain, Y493H shows lower RMSD value as compared to the other cases. (c) In BTB-domain, Y493H have three different peaks with broader distribution as a comparison to other structures. (d) The loop region shows two peaks and a high deviation in the structure.

It has been further revealed that a non-covalent inter-domain hydrogen-interaction between the residue His493 and Glu426 makes the structure more compact (Fig.4a). The probability distribution curve indicates that the average value for the interaction is 3.38Å which is almost more inclined to the formation of the hydrogen bond (Fig.4b). We have not found a similar interaction in any other mutant and is also absent in WT (Fig.4c).

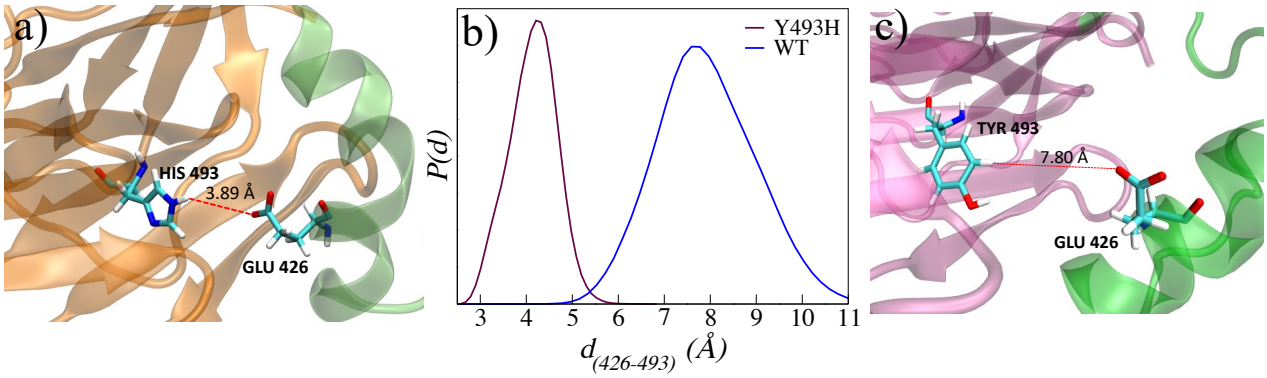

Figure 4: Non-covalent electrostatic interactions between the residues His493-Glu426 in Y493H. (a) Graphical representations of the hydrogen-interaction between His493 residue of Kelch-domain and Glu426 of BTB-domain in Y493H. (b) The probability distribution curve for the Y493H and WT along with the distance between Glu426-His493/Tyr493. (c) Graphical representational of the interaction in the WT which shows an absence of interaction between two residues

3.2 Comparison of individual residue fluctuation

The fluctuations of individual amino-acid residues are responsible for the overall dynamics of the protein. To quantify these fluctuations, the root-mean-square-fluctuations (RMSF) analysis is performed along the simulated trajectories. It is observed that in all the studied proteins the residues in the BTB-domain (350-442 residues) fluctuates significantly more compared to the Kelch-domain (443-726 residues) as shown in Fig.5. However, larger fluctuations are observed for the Y493H and C580Y compared to the other mutants and WT. It is also observed that the RMS fluctuations in the WT are the lowest compared to all the mutants, except R539T which shows similar dynamics as the WT.

We have observed that the large fluctuations in RMSF for Y493H and C580Y are primarily arising from 370 to 390 amino-acid residues that constitute the loop-regions of the BTB-domain (shown in inset box). Thus it is evident that the loop-regions of the two particular mutants dominate the protein dynamics. We realized this from the proteins RMSD analysis as well.

Comparing the protein dynamics between Y493H and C580Y, we realized that even

though both of them possess larger fluctuations in the loop regions but the microscopic origin of the protein dynamics is completely different from each other. In C580Y, Cys580 residue loses a hydrogen bond interaction with Gly533 (Fig.S3), while in the case of Y493H the additional hydrogen bond between His493 and Glu426 compacts the protein but with the cost of enhancing the fluctuations of 370 to 390 residues. We observed that the mutation affects the atomistic motion of the residues that are far from the mutated site.

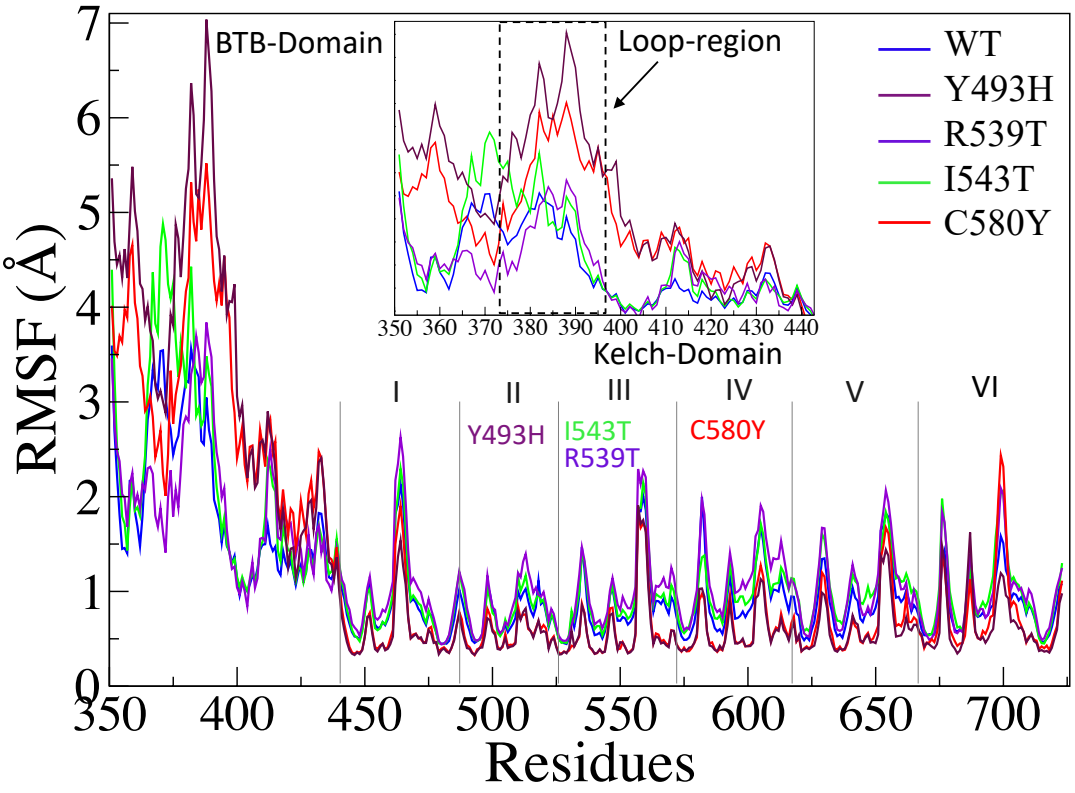

Figure 5: Calculated RMSF of WT and mutant cases where 350-442 residues correspond to the BTB-domain and 442-726 residues corresponds to the Kelch-domain. The BTB-domain showed higher fluctuations as compared to the Kelch domain. The higher fluctuations observed for the loop region of the BTB-domain and major peaks occur for the Y493H and C580Y mutants.

3.3 Secondary structure prediction

The secondary structure is a crucial component to study the structural behavior of the protein. We have performed the secondary structure analysis for all the cases and compared them with the WT. The secondary structure content is calculated only for the BTB-domain

(350-442 residues) as no structural deviation was observed for the Kelch domain.

The graphical representations of the secondary structures for all the cases are shown in Fig.6. It is observed that the loop-region, especially the 367-379 amino-acid residues of the BTB-domain shows the major difference in the structure, mainly in the Y493H. However, there is no large conformational differences are observed in between the 380 to 442 amino-acid residues except for Y493H, where the trend of secondary structure is changed around 416 to 421 amino-acid residues.

In WT, the secondary structure content of loop-region are primarily the mixture of turns and 3_{10}-helix especially from initial to 110 ns of the trajectory, afterwards this pattern changes to a mixture of turns and α-helix. To understand the conformational change in the loop-region the comparisons between the protein structures are performed. The structures obtained at different snapshots in the trajectory are superimposed to quantify the movement of loop-region. To do so, we have taken the snapshots at every 40ns interval from 0 to 200 ns and superimposed them together. We observed a quite nice superimposition of the structures only in the Kelch-domain not with the BTB-domain due to structural flexibility of the loop-region. The average change of positions for Gln391 (highest fluctuating residue in the loop-region) is approximately 10Å. (See Fig.S4 in SI)

In Y493H, three different conformations are obtained for the secondary structure. It forms turn and mixture of α-helix/3_{10}-helix from 0 to 85 ns, afterwards turn and 3_{10}-helix dominate up to 155ns. Then up to 200ns it is dominated by 3_{10}-helix and coils. The residues (417-422) which are close to the hydrogen-bond interaction region (His493-Glu426) is completely dominated by 3_{10}-helix, however, it forms turns in the WT. By superimposing the Y493H protein structures, the average distance obtained between the first and last structure is 29.92 Å which is larger than the 10 Å in WT (Fig.S5). The secondary structure change in the R539T is similar to the WT.

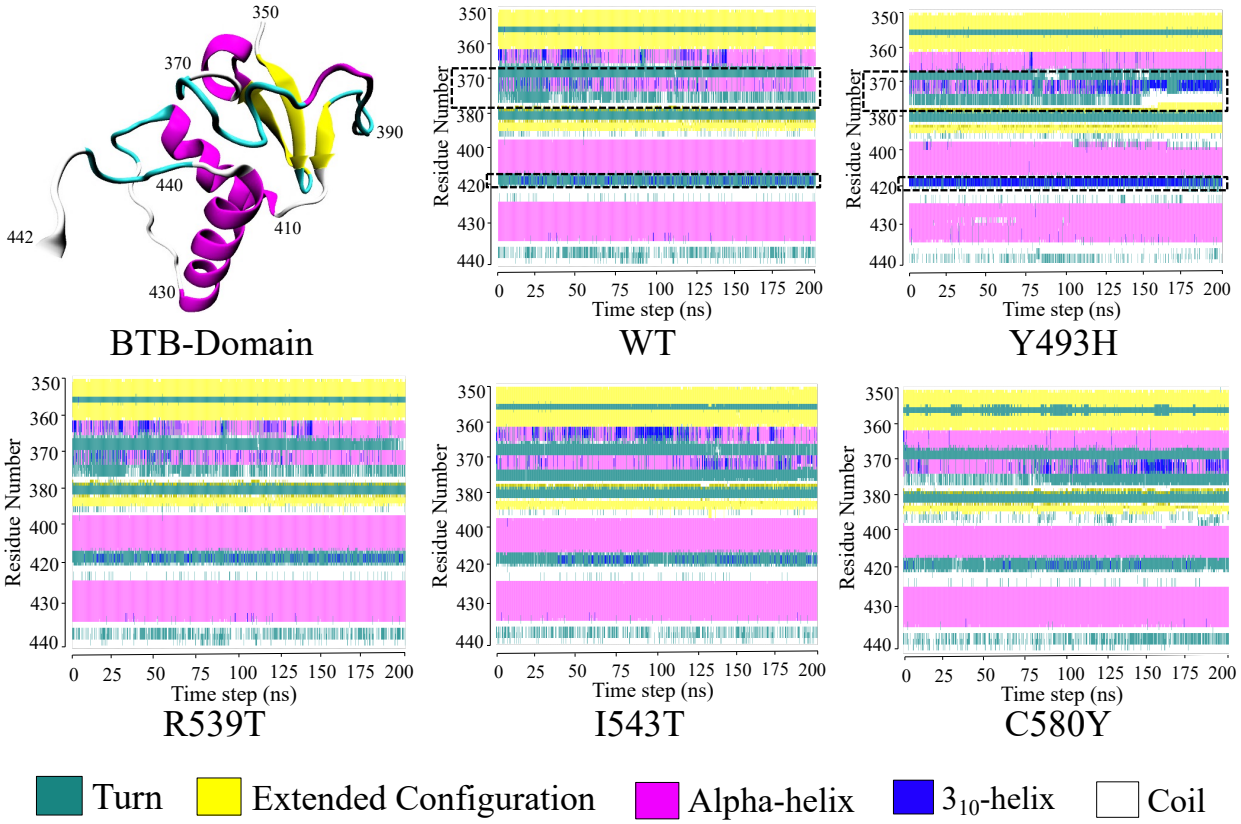

Figure 6: Calculated secondary structure analysis of BTB-domain in WT and mutant cases. The different structure elements are shown in colored boxes below the secondary structure map. The comparison of the structures shows that major structural changes occur in the loop-region, mainly in Y493H.

In C580y, the secondary structure consists of turns and α-helix from 0 to 83 ns, afterwards, it is dominated by turns and a mixture of α-helix and 3_{10}-helix. Comparison of the average distance between the loop-region, we obtained the value of 11.94, 14.18 and 23.08 Å for the R539T, I543T and C580Y mutants respectively.

We observed that there is large change in the overall secondary structure of Y493H. Three different conformations are observed in the loop-region of the BTB-domain. The loop-region is dominated by the turn while it changes to the coil as the simulation proceeds. We have seen that the residues 417-422 are completely dominated by the 3_{10}-helix in Y493H. This pattern of secondary structure is not observed in any other mutants. It indicates that mutation in the Y493H has large impact on the secondary structure as compared to the other mutants.

3.4 Dynamic Cross-correlation matrix (DCCM)

Its been observed that a single mutation in the Kelch-domain can incite significant dynamical fluctuations in the BTB-domain but it is not clear how the fluctuations of the individual residues are correlated with each other especially those are residing far apart. A proper understanding of the correlated motions can shed light on the long-range interaction patterns and eventually at the allosteric behaviors.[38,49,50]

To harness the correlated behaviors of the residues, we have performed the dynamical cross-correlation matrices (DCCMs) analysis by computing all the Pearson cross-correlation coefficients for the backbone Cα atoms of all the residues. The DCCM maps for the WT, Y493H and C580Y are graphically presented in Fig.7 as we have observed the fluctuations in these mutants. However, the DCCM map for the other two mutants is shown in Fig.S6. The correlation matrix for the complete protein is shown in panel a and zoomed view of the BTB-domain is shown in panel b. The cyan and magenta colors depict the correlation and anti-correlation respectively, while white space depicts non-correlation dynamical behaviors between the residues.

For the BTB-domain, we have found a very interesting pattern in between the residues 350-370 (Fig.7b). The correlation behavior in this region is nearly similar for all the cases. The two positive correlations are crossing diagonally each other which is a rare phenomenon observed for this particular region. Correlation is found between residues 350-355 and 360-370 however, the uncorrelation is observed among the residues 355-360. This is the region that forms the turns in the secondary structure. The residues 370-390 (red-dotted region) have anti-correlation in the WT however, in the Y493H and C580Y the anti-correlation behavior is getting disrupted and uncorrelated motions in between the residues is dominated.

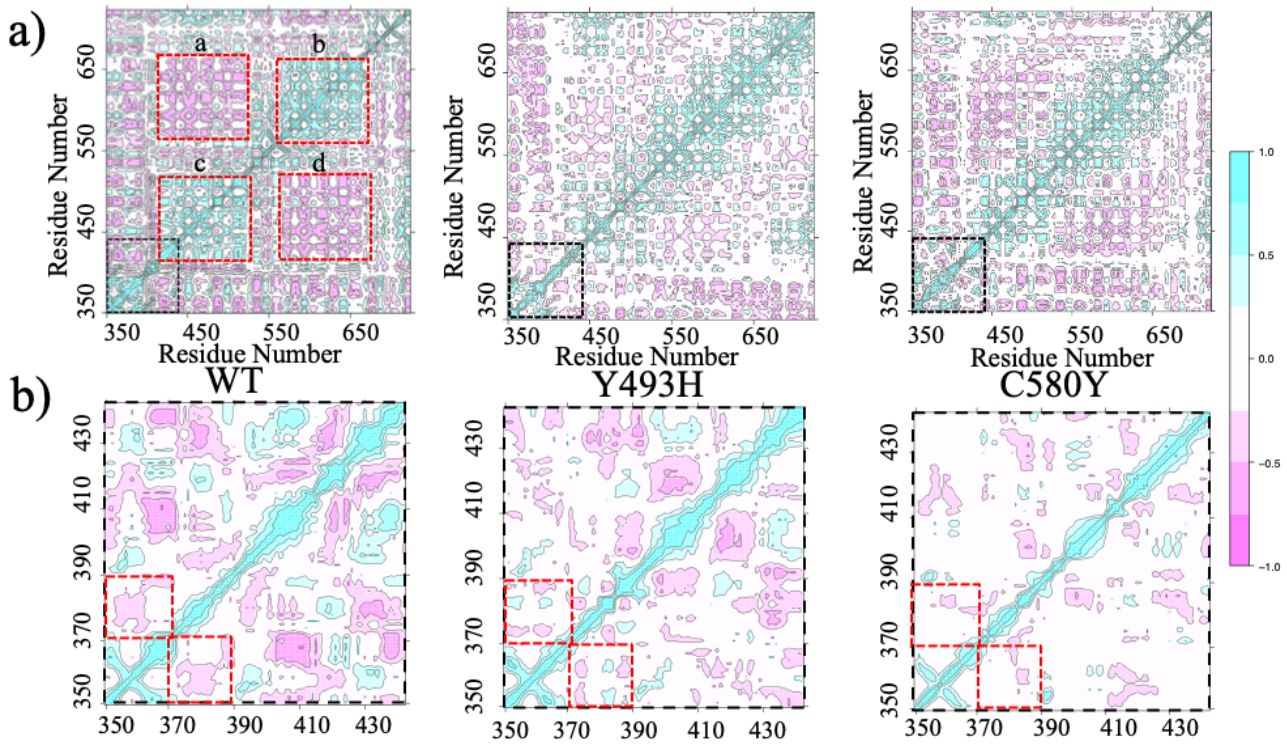

Figure 7: The Dynamics cross-correlations maps (DCCMs) for the WT, Y493H and C580Y mutants obtained from the entire production dynamics. The black dotted region (residues 350-442) indicates the BTB domain and the zoomed view is shown in panel b. Color Code: cyan color bar belongs to the (positive) correlation, magenta is for anti-correlation and white depicts uncorrelation. In the WT there is correlation within the residue however, significantly increased anti-correlation or uncorrelation in the mutants.

Further, we look into the complete-protein region of the WT and compare it with the mutant proteins (Fig.7a). In the WT we observed the strong correlation between the protein residues 420-538 and 560-685 as shown in box c and b respectively. The strong anti-correlation behaviour is observed for the residues 565-690 (shown in box a and d). This pattern of correlation is completely disturbed for the mutant cases. Hence it is quite evident that the mutation reduce the correlations among the residues . It further indicates that the mutations affect the long range dynamical correlation and affect the overall protein dynamics of the residues.

4 Conclusions & Outlook

We have performed the classical molecular dynamics simulation of the *Pf*K13 protein that has been associated with the ubiquitination process and antimalarial drug resistance. The protein dynamics of the WT and four mutants i.e. Y493H, R539T, I543T and C580Y have been performed and compared with each other. We have observed that despite being in the mutated site structural dynamics of Kelch-domain remain almost same for all the cases as of WT. However, we have realized that mutation in the Kelch-domain instigates larger structural fluctuation in the BTB-domain. Further, it has been noticed that specifically, the loop region of the BTB domain is the primary reason for the large fluctuation.

Among all the mutants, the largest deviations in the dynamics occur only for the Y493H and C580Y. The non-covalent electrostatic His493-Glu426 interaction, as well as the secondary structure change, is also responsible for the large dynamical fluctuations in Y493H. However, the absence of non-covalent intradomain interaction (Cys580-Gly533) causes the higher fluctuations in C580Y. The mutations also change the dynamical cross-correlation matrix pattern of the residues and break the interdomain correlation in the proteins. In a nutshell, the mutations in Kelch domain enhances the structural fluctuations in the BTB-domain that binds with cullin protein. Could the large fluctuations of the BTB-domain of the mutants be the reason for antimalarial drug resistance?

Probably yes, as the BTB-domain associates with the cullin protein to regulate the ubiquitination of the substrate protein. The enhanced dynamical fluctuations of the BTB-domain will hamper the binding interaction between the cullin protein and *Pf*K13 protein. This implies that disruption in the binding interaction will probably hinder the process of ubiquitination and cause the drug resistance in the mutant protein. However, this computational outcome is yet to be verified through plausible experimental studies.

Acknowledgement

The authors thank Aashish Bhatt for various helpful discussions and acknowledge the financial support from the Department of Science and Technology through SERB-CRG project no. CRG/2019/003237 and Indo-Sweden joint project no. DST/INT/SWD/VR/P-01/2016. The Ph.D. fellowship support and computational resources provides by the Institute of Nano Science and Technology (INST) are highly acknowledged.

References

(1) Turschner, S.; Efferth, T. Drug resistance in Plasmodium: natural products in the fight against malaria. *Mini-Rev. Med. Chem.* **2009**, *9*, 206–214.

(2) Dondorp, A. M.; Fairhurst, R. M.; Slutsker, L.; MacArthur, J. R.; MD, J. G. B.; Guerin, P. J.; Wellems, T. E.; Ringwald, P.; Newman, R. D.; Plowe, C. V. The threat of artemisinin-resistant malaria. *New. Engl. J. Med.* **2011**, *365*, 1073–1075.

(3) Fairhurst, R. M.; Nayyar, G. M.; Breman, J. G.; Hallett, R.; Vennerstrom, J. L.; Duong, S.; Ringwald, P.; Wellems, T. E.; Plowe, C. V.; Dondorp, A. M. Artemisinin-resistant malaria: research challenges, opportunities, and public health implications. *Am. J. Trop. Med. Hyg.* **2012**, *87*, 231–241.

(4) Dhorda, M.; Amaratunga, C.; Dondorp, A. M. Artemisinin and multidrug-resistant Plasmodium falciparum–a threat for malaria control and elimination. *Curr. Opin. Infect. Dis.* **2021**, *34*, 432.

(5) Amaratunga, C.; Witkowski, B.; Khim, N.; Menard, D.; Fairhurst, R. M. Artemisinin resistance in Plasmodium falciparum. *Lancet Infect. Dis.* **2014**, *14*, 449–450.

(6) Fairhurst, R. M.; Dondorp, A. M. Artemisinin-resistant Plasmodium falciparum malaria. *Microbiol. Spectr.* **2016**, *4*, 4–3.

(7) Dondorp, A. M.; Nosten, F.; Yi, P.; Das, D.; Phyo, A. P.; Tarning, J.; Lwin, K. M.; Ariey, F.; Hanpithakpong, W.; Lee, S. J., et al. Artemisinin resistance in Plasmodium falciparum malaria. *New. Engl. J. Med.* **2009**, *361*, 455–467.

(8) Ashley, E. A.; Dhorda, M.; Fairhurst, R. M.; Amaratunga, C.; Lim, P.; Suon, S.; Sreng, S.; Anderson, J. M.; Mao, S.; Sam, B., et al. Spread of artemisinin resistance in Plasmodium falciparum malaria. *New. Engl. J. Med.* **2014**, *371*, 411–423.

(9) Phyo, A. P.; Nkhoma, S.; Stepniewska, K.; Ashley, E. A.; Nair, S.; McGready, R.; ler Moo, C.; Al-Saai, S.; Dondorp, A. M.; Lwin, K. M., et al. Emergence of artemisinin-resistant malaria on the western border of Thailand: a longitudinal study. *Lancet.* **2012**, *379*, 1960–1966.

(10) Thriemer, K.; Hong, N. V.; Rosanas-Urgell, A.; Phuc, B. Q.; Ha, D. M.; Pockele, E.; Guetens, P.; Van, N. V.; Duong, T. T.; Amambua-Ngwa, A., et al. Delayed parasite clearance after treatment with dihydroartemisinin-piperaquine in Plasmodium falciparum malaria patients in central Vietnam. *Antimicrob. Agents Chemother.* **2014**, *58*, 7049–7055.

(11) Hien, T. T.; Thuy-Nhien, N. T.; Phu, N. H.; Boni, M. F.; Thanh, N. V.; Nha-Ca, N. T.; Thai, C. Q.; Van Toi, P.; Thuan, P. D.; Merson, L., et al. In vivo susceptibility of Plasmodium falciparum to artesunate in Binh Phuoc Province, Vietnam. *Malar. J.* **2012**, *11*, 1–11.

(12) Kyaw, M. P.; Nyunt, M. H.; Chit, K.; Aye, M. M.; Aye, K. H.; Aye, M. M.; Lindegardh, N.; Tarning, J.; Imwong, M.; Jacob, C. G., et al. Reduced susceptibility of Plasmodium falciparum to artesunate in southern Myanmar. *PLoS One.* **2013**, *8*, e57689.

(13) Huang, F.; Takala-Harrison, S.; Jacob, C. G.; Liu, H.; Sun, X.; Yang, H.; Nyunt, M. M.; Adams, M.; Zhou, S.; Xia, Z., et al. A single mutation in K13 predominates in southern

China and is associated with delayed clearance of Plasmodium falciparum following artemisinin treatment. *J. Infect. Dis.* **2015**, *212*, 1629–1635.

(14) Das, S.; Saha, B.; Hati, A. K.; Roy, S. Evidence of artemisinin-resistant Plasmodium falciparum malaria in Eastern India. *New. Engl. J. Med.* **2018**, *379*, 1962–1964.

(15) Mishra, N.; Prajapati, S. K.; Kaitholia, K.; Bharti, R. S.; Srivastava, B.; Phookan, S.; Anvikar, A. R.; Dev, V.; Sonal, G. S.; Dhariwal, A. C., et al. Surveillance of artemisinin resistance in Plasmodium falciparum in India using the kelch13 molecular marker. *Antimicrob. Agents Chemother.* **2015**, *59*, 2548–2553.

(16) Rosenthal, P. J. Artemisinin resistance outside of Southeast Asia. *Am. J. Trop. Med. Hyg.* **2018**, *99*, 1357.

(17) Roper, C.; Alifrangis, M.; Ariey, F.; Talisuna, A.; Menard, D.; Mercereau-Puijalon, O.; Ringwald, P. Molecular surveillance for artemisinin resistance in Africa. *Lancet Infect. Dis.* **2014**, *14*, 668–670.

(18) Talisuna, A. O.; Karema, C.; Ogutu, B.; Juma, E.; Logedi, J.; Nyandigisi, A.; Mulenga, M.; Mbacham, W. F.; Roper, C.; Guerin, P. J., et al. Mitigating the threat of artemisinin resistance in Africa: improvement of drug-resistance surveillance and response systems. *Lancet Infect. Dis.* **2012**, *12*, 888–896.

(19) Straimer, J.; Gnädig, N. F.; Witkowski, B.; Amaratunga, C.; Duru, V.; Ramadani, A. P.; Dacheux, M.; Khim, N.; Zhang, L.; Lam, S., et al. K13-propeller mutations confer artemisinin resistance in Plasmodium falciparum clinical isolates. *Science.* **2015**, *347*, 428–431.

(20) Fairhurst, R. M. Understanding artemisinin-resistant malaria: what a difference a year makes. *Curr. Opin. Infect. Dis.* **2015**, *28*, 417.

(21) Ariey, F.; Witkowski, B.; Amaratunga, C.; Beghain, J.; Langlois, A.-C.; Khim, N.; Kim, S.; Duru, V.; Bouchier, C.; Ma, L., et al. A molecular marker of artemisinin-resistant Plasmodium falciparum malaria. *Nature.* **2014**, *505*, 50–55.

(22) Dafalla, O. M.; Alzahrani, M.; Sahli, A.; Al Helal, M. A.; Alhazmi, M. M.; Noureldin, E. M.; Mohamed, W. S.; Hamid, T. B.; Abdelhaleem, A. A.; Hobani, Y. A., et al. Kelch 13-propeller polymorphisms in Plasmodium falciparum from Jazan region, southwest Saudi Arabia. *Malar. J.* **2020**, *19*, 1–9.

(23) Anderson, T. J.; Nair, S.; McDew-White, M.; Cheeseman, I. H.; Nkhoma, S.; Bilgic, F.; McGready, R.; Ashley, E.; Pyae Phyo, A.; White, N. J., et al. Population parameters underlying an ongoing soft sweep in Southeast Asian malaria parasites. *Mol. Biol. Evol.* **2017**, *34*, 131–144.

(24) Ménard, D.; Khim, N.; Beghain, J.; Adegnika, A. A.; Shafiul-Alam, M.; Amodu, O.; Rahim-Awab, G.; Barnadas, C.; Berry, A.; Boum, Y., et al. A worldwide map of Plasmodium falciparum K13-propeller polymorphisms. *New. Engl. J. Med.* **2016**, *374*, 2453–2464.

(25) Singh, G. P.; Goel, P.; Sharma, A. Structural mapping of Kelch13 mutations associated with artemisinin resistance in malaria. *J. Struct. Funct. Genomics.* **2016**, *17*, 51–56.

(26) Ghorbal, M.; Gorman, M.; Macpherson, C. R.; Martins, R. M.; Scherf, A.; Lopez-Rubio, J.-J. Genome editing in the human malaria parasite Plasmodium falciparum using the CRISPR-Cas9 system. *Nat. Biotechnol.* **2014**, *32*, 819–821.

(27) Taylor, S. M.; Parobek, C. M.; DeConti, D. K.; Kayentao, K.; Coulibaly, S. O.; Greenwood, B. M.; Tagbor, H.; Williams, J.; Bojang, K.; Njie, F., et al. Absence of putative artemisinin resistance mutations among Plasmodium falciparum in sub-Saharan Africa: a molecular epidemiologic study. *J. Infect. Dis.* **2015**, *211*, 680–688.

(28) Geyer, R.; Wee, S.; Anderson, S.; Yates III, J.; Wolf, D. A. BTB/POZ domain proteins are putative substrate adaptors for cullin 3 ubiquitin ligases. *Mol. cell.* **2003**, *12*, 783–790.

(29) Chen, H.-Y.; Chen, R.-H. Cullin 3 ubiquitin ligases in cancer biology: functions and therapeutic implications. *Front. Oncol.* **2016**, *6*, 113.

(30) Zhang, D. D.; Lo, S.-C.; Cross, J. V.; Templeton, D. J.; Hannink, M. Keap1 is a redox-regulated substrate adaptor protein for a Cul3-dependent ubiquitin ligase complex. *Mol. Cell. Biol.* **2004**, *24*, 10941–10953.

(31) Pinkas, D. M.; Sanvitale, C. E.; Bufton, J. C.; Sorrell, F. J.; Solcan, N.; Chalk, R.; Doutch, J.; Bullock, A. N. Structural complexity in the KCTD family of Cullin3-dependent E3 ubiquitin ligases. *Biochem. J.* **2017**, *474*, 3747–3761.

(32) Prag, S.; Adams, J. C. Molecular phylogeny of the kelch-repeat superfamily reveals an expansion of BTB/kelch proteins in animals. *BMC Bioinform.* **2003**, *4*, 1–20.

(33) Canning, P.; Cooper, C. D.; Krojer, T.; Murray, J. W.; Pike, A. C.; Chaikuad, A.; Keates, T.; Thangaratnarajah, C.; Hojzan, V.; Marsden, B. D., et al. Structural basis for Cul3 protein assembly with the BTB-Kelch family of E3 ubiquitin ligases. *J. Biol. Chem.* **2013**, *288*, 7803–7814.

(34) Adams, J.; Kelso, R.; Cooley, L. The kelch repeat superfamily of proteins: propellers of cell function. *Trends Cell Biol.* **2000**, *10*, 17–24.

(35) Mbengue, A.; Bhattacharjee, S.; Pandharkar, T.; Liu, H.; Estiu, G.; Stahelin, R. V.; Rizk, S. S.; Njimoh, D. L.; Ryan, Y.; Chotivanich, K., et al. A molecular mechanism of artemisinin resistance in Plasmodium falciparum malaria. *Nature.* **2015**, *520*, 683–687.

(36) Haldar, K.; Bhattacharjee, S.; Safeukui, I. Drug resistance in Plasmodium. *Nat. Rev. Microbiol.* **2018**, *16*, 156–170.

(37) Suresh, N.; Haldar, K. Mechanisms of artemisinin resistance in Plasmodium falciparum malaria. *Curr Opin Pharmacol.* **2018**, *42*, 46–54.

(38) Bhatt, A.; Ali, M. E. Understanding the role of R266K mutation in cystathionine β-synthase (CBS) enzyme: an in silico study. *J. Biomol. Struct. Dyn.* **2021**, 1–9.

(39) Bisht, A.; Sharma, M.; Sharma, S.; Ali, M. E.; Panda, J. J. Carrier-free self-built aspirin nanorods as anti-aggregation agents towards alpha-crystallin-derived peptide aggregates: potential implications in non-invasive cataract therapy. *J. Mater. Chem. B.* **2019**, *7*, 6945–6954.

(40) Kour, A.; Sharma, S.; Dube, T.; Bisht, A.; Sharma, M.; Mishra, J.; Ali, M. E.; Panda, J. J. l-3, 4-Dihydroxyphenylalanine templated anisotropic gold nano/micro-roses as potential disrupters/inhibitors of α-crystallin protein and its gleaned model peptide aggregates. *Int. J. Biol. Macromol.* **2020**, *163*, 2374–2391.

(41) Jiang, D.; Tempel, W.; Loppnau, P.; Graslund, S.; He, H.; Ravichandran, M.; Seitova, A.; Arrowsmith, C.; Edwards, A.; Bountra, C., et al. Crystal structure analysis of Kelch protein from Plasmodium falciparum. *PDB https://www. rcsb. org/structure/4ZGC (accession no. 4ZGC)* **2015**,

(42) DeLano, W. L., et al. Pymol: An open-source molecular graphics tool. *CCP4 Newsletter on protein crystallography* **2002**, *40*, 82–92.

(43) Nelson, M. T.; Humphrey, W.; Gursoy, A.; Dalke, A.; Kalé, L. V.; Skeel, R. D.; Schulten, K. NAMD: a parallel, object-oriented molecular dynamics program. *Int. J. High Perform. Comput. Appl.* **1996**, *10*, 251–268.

(44) Coppée, R.; Jeffares, D. C.; Miteva, M. A.; Sabbagh, A.; Clain, J. Comparative structural and evolutionary analyses predict functional sites in the artemisinin resistance malaria protein K13. *Sci. Rep.* **2019**, *9*, 1–17.

(45) Maier, J. A.; Martinez, C.; Kasavajhala, K.; Wickstrom, L.; Hauser, K. E.; Simmerling, C. ff14SB: improving the accuracy of protein side chain and backbone parameters from ff99SB. *J. Chem. Theory Comput.* **2015**, *11*, 3696–3713.

(46) Mark, P.; Nilsson, L. Structure and dynamics of the TIP3P, SPC, and SPC/E water models at 298 K. *J. Phys. Chem. A*. **2001**, *105*, 9954–9960.

(47) Darden, T.; York, D.; Pedersen, L. Particle mesh Ewald: An N log (N) method for Ewald sums in large systems. *J. Chem. Phys.* **1993**, *98*, 10089–10092.

(48) Humphrey, W.; Dalke, A.; Schulten, K. VMD: visual molecular dynamics. *J. Mol. Graph.* **1996**, *14*, 33–38.

(49) Bingol, E. N.; Sercinoglu, O.; Ozbek, P. Unraveling the Allosteric Communication Mechanisms in T-Cell Receptor–Peptide-Loaded Major Histocompatibility Complex Dynamics Using Molecular Dynamics Simulations: An Approach Based on Dynamic Cross Correlation Maps and Residue Interaction Energy Calculations. *J. Chem. Inf. Model.* **2021**, *61*, 2444–2453.

(50) Kasahara, K.; Fukuda, I.; Nakamura, H. A novel approach of dynamic cross correlation analysis on molecular dynamics simulations and its application to Ets1 dimer–DNA complex. *PloS one.* **2014**, *9*, e112419.

Graphical TOC Entry